Modulation of Photoactive Nanocomposite Cu Doped SnO₂ Anchored on G-C₃N₄ Polymeric Sheets by Green Synthesis and Degradation of Dye Malachite Green

Snigdha Dwivedi (iD)
Babasaheb Bhimrao Ambedkar University, India

Gajanan Pandey (iD)
Babasaheb Bhimrao Ambedkar University, India

To cite this article:

Modulation of Photoactive Nanocomposite Cu Doped SnO$_2$ Anchored on G-C$_3$N$_4$ Polymeric Sheets by Green Synthesis and Degradation of Dye Malachite Green

Snigdha Dwivedi, Gajanan Pandey

Abstract

Wastewater containing harmful dyes such as Malachite green poses a significant environmental challenge because of its high levels of carcinogenicity, mutagenicity, and toxicity. To address this issue, we developed a photocatalyst consisting of Cu doped SnO$_2$ nanocomposite supported onto g-C$_3$N$_4$ using green synthesis method with the assistance of *Murraya paniculata* leaves extract. To know about the structural, morphological chemical composition of the synthesized heterojunction several techniques of characterization techniques were employed such as XPS, XRD, BET, HRTEM, FESEM, EDAX and UV-Vis spectra. XRD results shows the spherical shape of the particles with the mean grain size of 2.18 and 2.14 nm for Cu doped SnO$_2$ and Cu doped SnO$_2$/g-C$_3$N$_4$ respectively. HRTEM results reveal that the fabricated Cu doped SnO$_2$ shows formation of very small size spherical nanoparticles. The heterojunction Cu doped SnO$_2$/g-C$_3$N$_4$ showed 2-D sheeted structure of g-C$_3$N$_4$ which acts as a translucent layer that captured sphere shaped Cu doped SnO$_2$ NPs. The XPS analysis verifies the existence of Sn, Cu, O, C and N in the synthesized heterojunction. The UV-Visible spectra helped to demonstrate the effective inhibition of plasmonic exciton annihilation within the heterojunction nanocomposite. When exposed to solar light, the designed nanocomposite heterojunction exhibited superior photocatalytic activity in the degradation of MG compared to undoped g-C$_3$N$_4$ and Cu doped SnO$_2$ binary nanocomposite. Radical scavenging studies indicated that •O2– radicals were the principle species accountable for the degradation of MG by the nanocomposite heterojunction. The dye MG photodegraded with pseudo-first order kinetics. The excellent photocatalytic performance and recyclability of nanocomposite can be attributed to its greater surface area, improved separation efficiency of excited e--h+ pairs and superior absorption of visible light.

Introduction

Contamination of water has emerged as a significant contemporary challenge which is primarily driven by the widespread use of chemicals in various industries and agricultural practices. The indiscriminate application of chemicals, including fertilizers and insecticides, in agricultural fields has led to the degradation of soil quality.

The repercussions of these toxic chemicals, accumulating in water bodies, pose a serious threat to aquatic ecosystems (Lai, 2017; Wen et al., 2021). In addressing water pollution, photocatalytic decontamination by nanomaterials has gained considerable attention due to its economic viability, scalability, and straightforward operational procedures. Many material scientists and engineers have focused a great deal of attention on nanocomposites among nanomaterials because of their many advantages over conventional materials. Engineered nano heterojunctions inherent interfacial potential barriers, such as those between metal oxide and metal oxide metal oxide and metal sulphide, Nobel metal and metal oxide, and metal oxide and carbon nanomaterials. These barriers play a crucial role in impeding the photogenerated charge carriers recombination, cooperatively, enhancing the photocatalytic properties of heterojunction nano catalysts(Alalm et al., 2021).

The continuous advancement in the synthesis of metal oxide nanostructures due to their adjustable particle size, crystallinity, and various associated properties, is driven by their versatile applications in technology. The key advantage of utilizing nano metal-oxide particles lies in the ease with which their characteristics can be modified and precisely regulated by incorporating appropriate dopants. Despite their promise, creation and design of innovative multicomponent nano heterojunctions present obstacles, including ensuring chemical stability and compatibility with band structures, and navigating complex multistep synthetic strategies. Overcoming these challenges is essential for fabricating efficient nano heterojunction catalysts for environmental remediation applications (Mohanta & Ahmaruzzaman, 2021). Metal oxides serve as the foundation for functional materials, showcasing distinct properties and a wide range of technological applications. Metal oxide semiconductors (MOSs), distinguished by their unique physical and chemical attributes, have garnered significant research attention due to their versatile potential in nanoelectronics, optoelectronics, photonics devices, spintronics devices, storage devices, and catalytic processes(Goswami et al., 2022). Transition metal oxides, such as SnO_2, ZnO, TiO_2, and WO_3, commonly employed as nano materials, exhibit distinctive physicochemical properties that make them suitable for enhancing the performance of optical and electronic devices.

Tin oxide nanostructured materials stand out as promising components in multiphase nano heterojunction water decontamination photocatalysts, given their tunable band gap, cost-effectiveness, low toxicity, and abundant availability (Mohanta & Ahmaruzzaman, 2016). Among these, SnO_2 stands out as a semiconductor material with wide band gap and energy gap (Eg) of 3.6 eV and a conduction band of n-type. Its intrinsic band gap defects have led to extensive applications in various fields, including the synthesis of photo-catalysts and oxidation catalysts(Kolmakov et al., 2003). Recognized for its exceptional optical and electrical properties, SnO_2 also demonstrates outstanding mechanical and chemical stability(Bamsaoud et al., 2011). The band arrangements in nanostructures of tin oxide can be modified through techniques such as ion doping, morphological adjustments, or composite formation. These modifications in the electronic surroundings of nanostructured materials made up of tin oxide have the potential to enhance the catalyst ability to capture light and impede the photogenerated exciton recombination. Consequently, this facilitates efficient photocatalytic properties(Chen et al., 2019; Li et al., 2020). The significance of metal oxide nanostructures with tunable sizes is steadily growing due to their remarkable properties and substantial technological applications. This heightened importance is underscored by the fact that the properties of metal-oxide materials can be easily customized and controlled through the addition of suitable dopants. (Hong et al., 2009; Kapilashrami et al., 2009; Kasar et al., 2008). Various methods have been

developed for synthesizing both doped and undoped SnO2 nanostructures, including spray pyrolysis, hydrothermal methods, polymer precursor techniques, evaporating tin grains in air, chemical vapor deposition, thermal evaporation of oxide powders, microwave-assisted solvothermal processes, magnetron sputtering, sonochemical methods, VLS method, laser ablation, rapid oxidation of elemental tin, co-precipitation method, and sol-gel method. Studies reveal that the addition of metal cations (Al, Co, Fe, and Cu) increases the surface area of SnO_2 nanoparticles(Jin et al., 2004).

Photocatalytic technologies, known for their eco-friendly nature, show promise in various environmental applications, including organic degradation, water treatment, reduction of heavy metal ions, and CO_2 reduction (Kumar et al., 2016; Zhao et al., 2020). SnO_2, employed for photocatalytic applications, has garnered significant attention due to its high oxidation potential, chemical inertness, long-term stability, non-toxicity, cost-effectiveness, and eco-friendly nature (Jiang et al., 2018; Kumar et al., 2017). However, the inherent photocatalytic properties of pristine SnO_2 face challenges, such as a large bandgap (3.6 eV) limiting absorption to the UV spectrum range and the electron-hole pairs recombination. To overcome these challenges, the bandgap can be tailored, and one effective approach is the doping of SnO_2. Doping SnO_2 with transition metals, such as Cu, enhances its optoelectronic properties like photoluminescence and optical band gap (Mishra et al., 2014). Doping of chemicals not only affects the conduction band but also tailors SnO_2 thin films optical band gap (Lee & Park, 2006). Recent literature reports highlight the doping of SnO_2 with various metals and semiconductors for diverse applications, with a specific focus in this study on Cu-doped SnO_2. Additionally, enhancing the stability and efficiency of photocatalyst of the Cu doped SnO_2 nanohybrid can be achieved by integrating it into a two-dimensional nanomaterial such as graphitic nitride (g-C_3N_4). Notably, g-C_3N_4, characterized by a narrow bandgap (2.7 eV), interacts effectively with visible light, generating excitons (Akhundi et al., 2020). The band structure suitability of g-C_3N_4 with Cu doped SnO_2 facilitates the smooth movement of photogenerated electrons across various conduction band levels, leading to increased separation of charge because of its potential junctions at the interfaces. The sp2-hybridized carbon structure of g-C_3N_4 serves as a supportive matrix, preventing the clustering of nanomaterials (Raha & Ahmaruzzaman, 2020). Moreover, the π-network inherent in the 2-D g-C_3N_4 nanosheet enhances the mobility charge in photogenerated carriers. Consequently, the integration of g-C_3N_4 with the Cu doped SnO_2 nanohybrid not only prevents SnO_2 photo corrosion but also enhances charge mobility stability, and imparts high mass diffusibility.

Experimental Section

Materials Required

We collected the fresh leaves of *Murraya paniculata* plant found on the Babasaheb Bhimrao Ambedkar University campus. These leaves, along with Melamine, Tin chloride dihydrate ($SnCl_2.2H_2O$), Copper sulphate ($CuSO_4$), and Malachite Green (MG), were used in our study. Additionally, various solvents and chemicals, including NaOH, HCl, ethanol, disodium EDTA, benzoquinone, ferroin indicator, isopropyl alcohol, $K_2Cr_2O_7$, Ag_2SO_4, $HgSO_4$, H_2SO_4, and Ferrous ammonium sulfate, all of which were of ACS grade, were employed without further purification.

Preparation of *Murraya Paniculata* Leaves Extract

In the process of modulating the Cu doped SnO_2 nanocomposite, an extract from the leaves of *Murraya paniculata* serves as a dual role, both stabilizing and reducing agent. To prepare this extract, fresh *Murraya paniculata* leaves underwent thorough washing with deionized water to eliminate any dust and impurities. Subsequently, the cleaned leaves were air-dried for seven days to retain their phytochemical properties. Once dried, the leaves were finely powdered. A total of 30 grams of this powdered *Murraya paniculata* material was mixed in 500 mL of double-distilled water and warmed at 80°C for 2 hours under reflux conditions. The resulting extract was then allowed to cool and subsequently filtered using Whatman filter paper No. 1.

Synthesis of Binary Nanocomposite Cu Doped SnO_2

To produce SnO_2 nanoparticles, 75 mL of *Murraya paniculata* leaf extract was added to 125 mL of a 0.5 mol solution of Tin chloride dihydrate ($SnCl_2.2H_2O$) dropwise. The mixture was consistently agitated on a magnetic stirrer at ambient temperature. After 5 hrs, the mixture was allowed to cool and then subjected to 30 minutes of sonication at 4000 rpm. The resulting precipitate was collected and underwent multiple washes with double-distilled water followed by ethanol. This white precipitate was then oven dried at 80°C for 2 hours and subsequently subjected to a muffle furnace at 650°C for 1 hour. For the synthesis of the binary nanocomposite Cu doped SnO_2, 10 ml of 0.2 mM solution of $CuSO_4$ was added to 75 mL of *Murraya paniculata* leaf extract. The mixture was continuously stirred on a magnetic stirrer at ambient temperature for 2 hours. In a separate container, 1g of the synthesized Molybdenum oxide nanoparticles was introduced to 100 mL of double-distilled water. Both solutions were blended and stirred continuously at room temperature for an additional 2 hours. The resulting precipitate was collected and subjected to several washes with deionised water and ethanol before being dried in an oven at 160°C.

Preparation of $g-C_3N_4$ Sheets

Pristine g-C3N4 sheets were produced by employing urea as the primary raw material in a thermal polycondensation process. This procedure began with the calcination of 15 grams of melamine in a muffle furnace, gradually raising the temperature to 550°C over a span of 3 hours. The resultant light-yellow $g-C_3N_4$ powder was subsequently finely ground and preserved for subsequent applications.

Synthesis of Cu Doped SnO_2/$g-C_3N_4$ Semiconductor Heterojunction

The Cu doped SnO_2/$g-C_3N_4$ semiconductor heterojunction was formed by introducing 1 gram of the synthesized pristine $g-C_3N_4$ to 100 mL of deionised water and subjected to sonication for one hr to ensure thorough dispersion. Subsequently, 0.5 grams of the synthesized binary nanocomposite Cu doped SnO_2 were introduced into the solution, followed by an additional two hours of sonication. The resulting Cu doped SnO_2/$g-C_3N_4$ semiconductor heterojunction was then collected and oven dried at 120°C.

Characterization

The photochemical activity of the synthesized pristine g-C_3N_4, the binary nanocomposite Cu doped SnO_2, and the Cu doped SnO_2/g-C_3N_4 semiconductor heterojunction, was assessed using a Carry 100 dual-beam UV-visible spectrophotometer. This evaluation covered a range of wavelengths spanning from 200 to 800 nm. To gain insight into the crystallinity and structure of the synthesized materials, XRD patterns were obtained using an X'pert Pro X-ray diffractometer from PANalytical in the Netherlands, which employed Ni-filtered Kα radiations. In order to look into the detailed dimensions and shape of the synthesized materials, field-emission scanning electron microscopy (FESEM) was performed using equipment from Carl Zeiss Microscopy Ltd., and Energy Dispersive X-ray analysis (EDAX) was conducted with a Team EDS system equipped with an Octane Plus SDD detector. High-resolution transmission electron microscope (HRTEM) images were captured by utilizing the Tecnai G2 20 TWIN instrument from FEI Company of the USA PTE, LTD to obtain microstructural insights into the synthesized materials. X-ray photoelectron spectroscopy (XPS) was carried out using the Thermo Fisher Scientific spectrometer, specifically the Kα model, to assess the chemical composition and oxidation state of the Cu doped SnO_2/g-C_3N_4 semiconductor heterojunction. The BET surface area analyzer, BELSORP mini II from Japan, was employed to determine the adsorption and desorption characteristics of nitrogen gas and to analyze the specific surface area of both the binary nanocomposite Cu doped SnO_2 and the Cu doped SnO_2/g-C_3N_4 heterojunction.

Photo Assisted Catalytic Degradation Experiments

There were photocatalysis experiments conducted under the influence of direct sunlight exposure. The catalysts tested in the photodegradation of Malachite green (MG) dye included the synthesized pristine g-C_3N_4, the binary nanocomposite Cu doped SnO_2, and the semiconductor Cu doped SnO_2/g-C_3N_4 heterojunction. The experimental setup involved dividing a 10 ppm MG dye solution into five separate Pyrex vials, each containing 50 mL of solution to ensure equal volumes. Variable amounts of catalyst (10, 20, 30, 40, and 50 mg) were added to each vial, and a blank vial was prepared by introducing 10 mL of MG dye solution without any catalyst. Equilibrium between adsorption and desorption was achieved by leaving the vials in darkness for 30 minutes.

After this dark period, the mixtures were kept in direct sunlight to initiate the photocatalytic degradation of MG dye. Throughout the process, time intervals were tracked for a total duration of 100 minutes utilizing a UV-Visible spectrophotometer. The concentration of MG dye was assessed at a wavelength of 617 nm during this process. Additionally, the impact of pH on the photodegradation of MG dye was investigated. The solution pH was altered and maintained within the range of 3 to 13 by adding dilute solutions of HCl and NaOH to the vials. To study the kinetics and rate constant of MG dye photodegradation, a graph was plotted between $\ln(C_0/C_t)$ and time, where C_t represents the final concentration of CV dye and C_0 is the initial concentration.

COD Measurement

To assess the COD and evaluate the photodegradation rate of harmful organic dyes under direct sunlight exposure, the dichromate reflux method was employed. This method involves subjecting both the treated and untreated

Malachite green (MG) dye to digestion in the presence of standard quantities of Ag_2SO_4, $K_2Cr_2O_7$, $HgSO_4$, and H_2SO_4 for a duration of 2 hours. Subsequently, the resulting mixture underwent titration using 0.1 N ferrous ammonium sulphate, aided by the addition of two to three Ferroin indicator drops. To establish a reference point, a blank titration was conducted using double-distilled water instead of the analytes. The COD of the prepared nanoparticle was calculated using the following formula:

$$COD = \frac{[(V_{blank} - V_{sol})] \times 8 \times 1000}{V_{sol}}$$

Here, V_{blank} represents the volume in mL of the titrant (0.1 N ferrous ammonium sulfate) required for the blank titration, V_{sol} represents the volume in mL of the titrant required for the sample titration, and 8 is a constant factor. Photo assisted degradation intermediate analysis by LC-MS

The characterization and identification of byproducts generated during the photo assisted catalytic decomposition of MG dye, facilitated by the Cu doped SnO_2/g-C_3N_4 semiconductor heterojunction as a catalyst, were performed through the application of LC-MS. LC-MS blends the mass analysis methods with the separation capabilities of liquid chromatography, providing a powerful method for chemical analysis. The LC-MS analysis was performed by utilizing an Agilent 1260 Infinity II instrument, with the temperature of the column continued at 25°C. The mobile phase was propelled through the system at a flow rate of 0.3 mL/min, and the entire analytical process spanned a duration of 9 minutes.

Radical Scavenger Experiment

To acquire a better understanding of the mechanism responsible for the decomposition of MG dye using the Cu doped SnO_2/g-C_3N_4 semiconductor heterojunction as a photocatalyst, radical trapping experiments were conducted. These experiments involved the use of scavenging agents like Isopropyl alcohol (IPA), p-benzoquinone (BQ), and disodium EDTA (Na2EDTA) to capture and neutralize specific radicals, namely hydroxyl radicals (•OH), superoxide radicals (•O2-), and positive holes (h+), respectively. These scavengers were sequentially introduced, and their interactions with the radicals were monitored through spectrophotometric measurements.

Recyclability of the Catalyst

To evaluate the durability and reusability of the Cu doped SnO_2/g-C_3N_4 semiconductor heterojunction employed in the photodegradation process, the catalyst was recovered, underwent a cleaning procedure using ethanol and acetone, and was then dried. This prepared composite was then employed for a total of four consecutive cycles.

Result and Discussion
X-ray Diffraction Analysis

XRD evaluation was conducted over the range of 20° to 90° to analyse the structure and purity of the prepared

crystalline materials. The X-ray diffraction patterns of the synthesized materials, including pristine g-C$_3$N$_4$, the binary nanocomposite Cu doped SnO$_2$, and the Cu doped SnO$_2$/g-C$_3$N$_4$ semiconductor heterojunction, are displayed in Fig. 1. In the X-ray diffraction pattern of pristine g-C3N4, characteristic peaks were observed at 12.91° and 27.28°, corresponding to the (100) and (002) crystallographic planes, correspondingly. These peaks indicated the inherent graphitic arrangement typical of carbon nitride-derived materials (JCPDS 00-87-1526) (Wang et al., 2009). The primary peaks in the X-ray diffraction pattern of the binary nanocomposite Cu doped SnO$_2$ are depicted in Fig 1(a). The diffraction peaks obtained at 26.49°, 33.68 °, 51.69 ° and 65.12 ° which corresponds to (110), (101), (211), and (310) crystallographic planes receptively confirms the presence of the tetragonal structure of SnO$_2$ (JCPDS 41-1445)(Li et al., 2020). No other peak indicating the presence of copper or other Cu including compounds had been observed from the XRD spectra which shows that the Cu^{2+} ions are incorporated successfully in the composite (Sagadevan et al., 2019). The X-ray diffraction patterns of the Cu doped SnO$_2$/g-C$_3$N$_4$ heterojunction featured diffraction peaks attributed to g-C$_3$N$_4$, and Cu doped SnO$_2$, confirming their coexistence. These XRD results illustrate how Cu doped SnO$_2$ interacts with and is distributed within the sheets of pristine g-C$_3$N$_4$. The mean grain size of Cu doped SnO$_2$ and Cu doped SnO$_2$/g-C$_3$N$_4$ was determined using the Debye-Scherer formula, *D = 0.89λ/βCosθ* which are found to be 2.18 and 2.14 nm respectively.
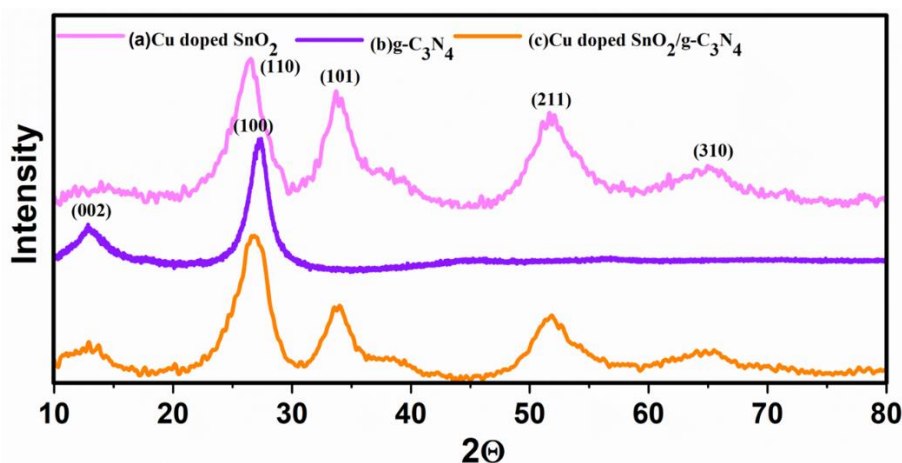

Figure 1. XRD Pattern of Cu Doped SnO$_2$ (a), g-C$_3$N$_4$ (b) and Cu Doped SnO$_2$/g-C$_3$N$_4$ (c)

Morphology Analysis

SEM analysis was employed to explore the structure and topology of Cu doped SnO$_2$ and Cu doped SnO$_2$/g-C$_3$N$_4$ materials synthesized through a green approach. The SEM images of Cu doped SnO$_2$ revealed the presence of small spherical particles that agglomerate to form larger aggregates (Fig 2 a-b).In contrast, Cu doped SnO$_2$/g-C$_3$N$_4$ SEM images (Fig 2 c-d) displayed tiny particles dispersed across g-C$_3$N$_4$ sheets. To gain deeper insights into the morphology, TEM and HR-TEM evaluation were conducted. TEM images of Cu doped SnO$_2$ showcased the formation of very small spherical nanoparticles, which agglomerate to form larger aggregates in the presence of phytochemicals from the plant extract, as observed in the SEM images (Fig 3 a-f). The HRTEM images (Fig 3e) revealed clear lattice fringes, confirming the crystalline nature of the nanoparticles with a d spacing of 0.33 nm according to the (110) plane of tetragonal SnO$_2$. For the Cu doped SnO$_2$/g-C$_3$N$_4$ heterojunction, TEM and HRTEM

images (Fig 4 a-f) depicted a 2-D sheeted structure of g-C_3N_4 acting as a translucent layer, capturing sphere-shaped Cu doped SnO_2 nanoparticles dispersed across the sheet. The interplanar spacing (0.333 nm) observed in HRTEM (Fig 4 e) matched that of Cu doped SnO_2, confirming the (110) plane of tetragonal SnO_2. The elemental mapping images of Cu doped SnO_2 revealed the existence of Sn, Cu, and O elements scattered throughout the structure (Fig 5 a-d). Similarly, Cu doped SnO_2/g-C_3N_4 Elemental mapping micrographs (Fig 6 a-f) displayed the random distribution of Sn, Cu, O, C, and N elements, confirming the successful synthesis of the heterojunction nanocomposite.
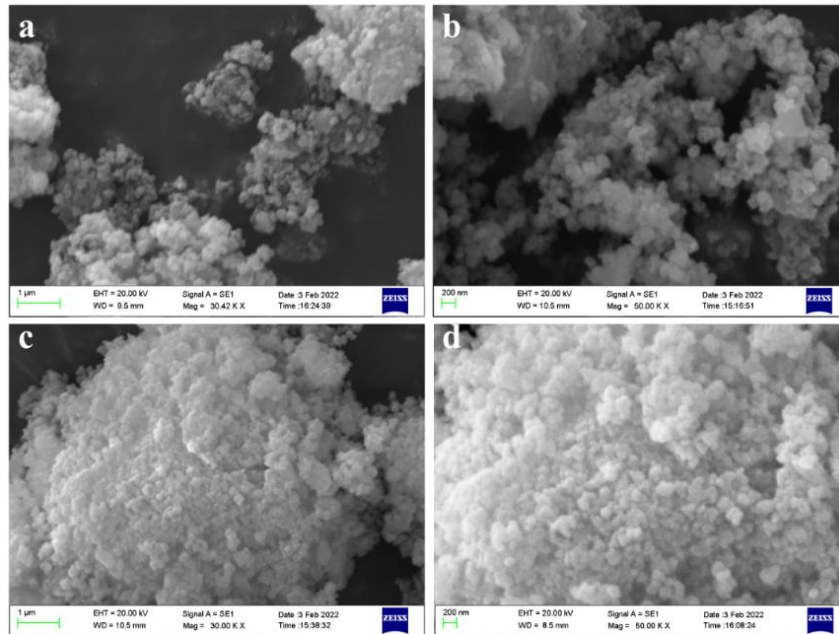
Figure 2. FESEM Images of Nanocomposite Cu Doped SnO_2 (a,b) and Cu Doped SnO_2/g-C_3N_4 Heterojunction (c,d)
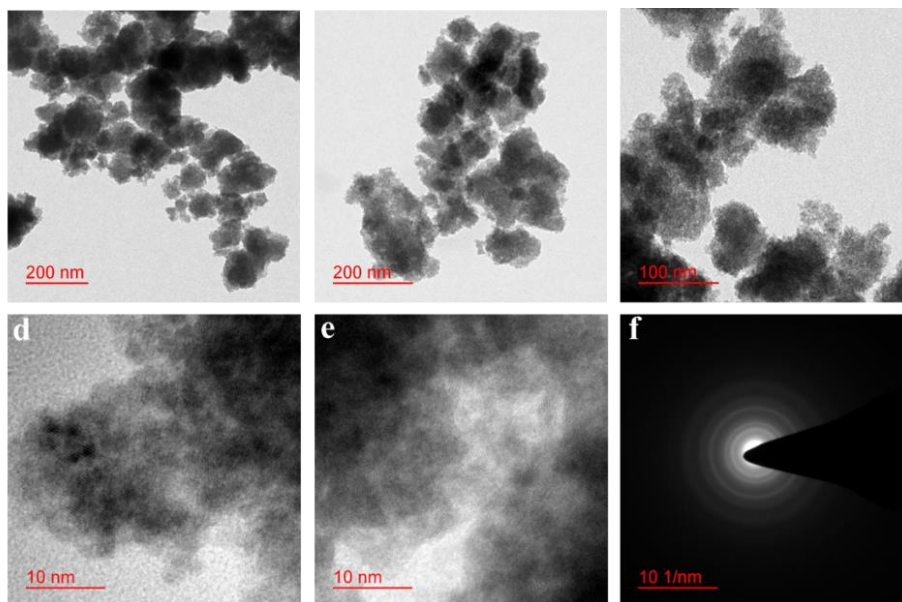

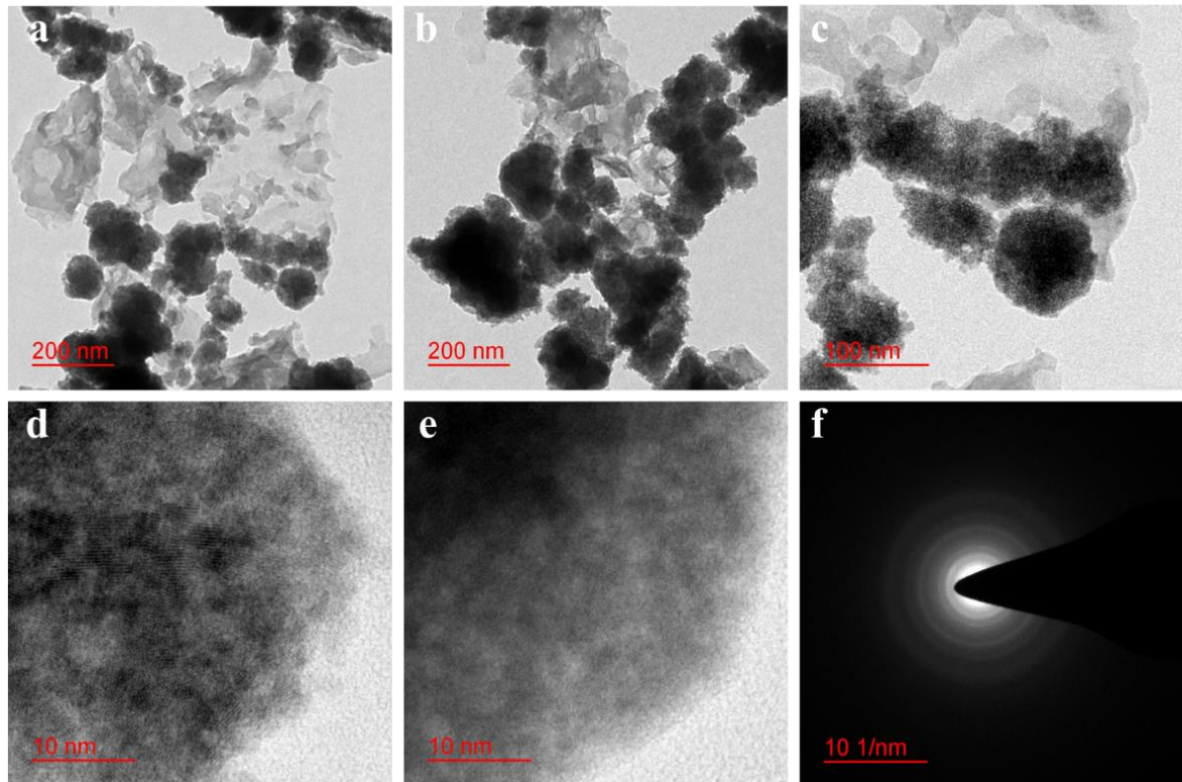Figure 3. TEM and HRTEM Images of Cu Doped SnO_2 Nanocomposite (a-f)

Figure 4. TEM and HRTEM Images of Cu Doped SnO_2/g-C_3N_4 Nanocomposite Heterojunction(a-f)
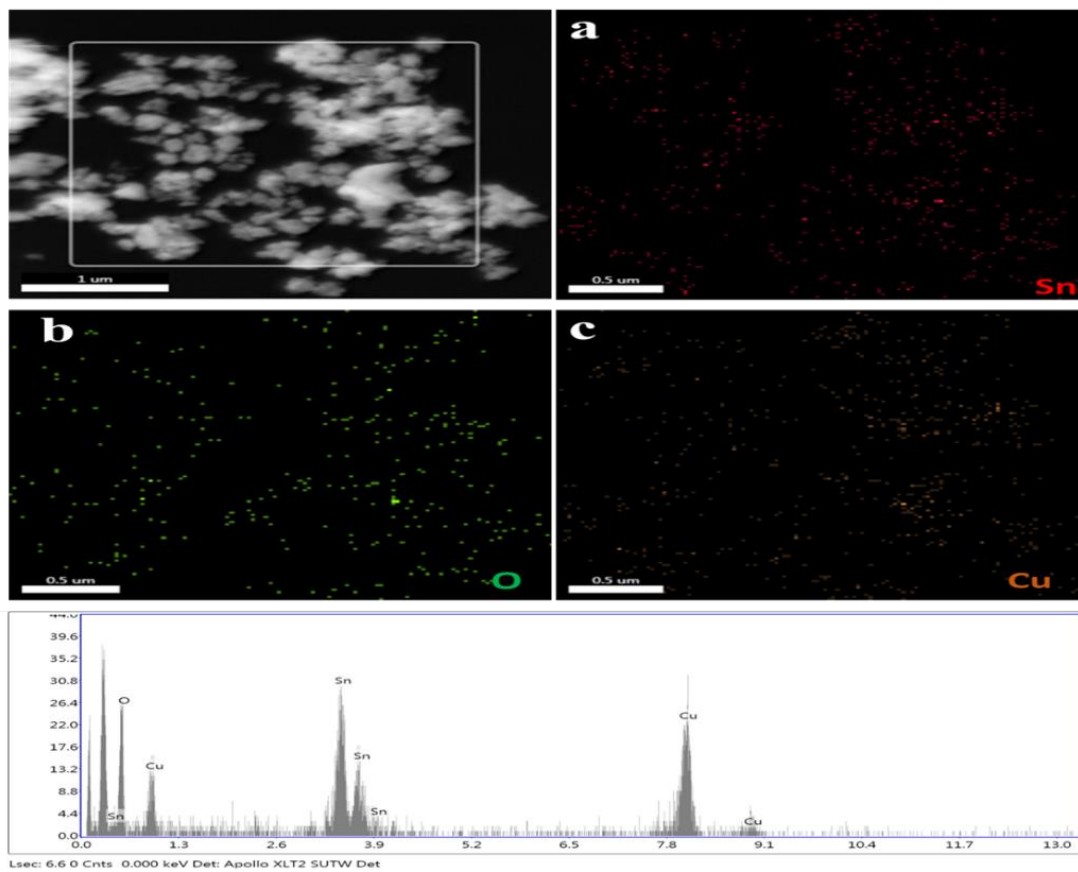

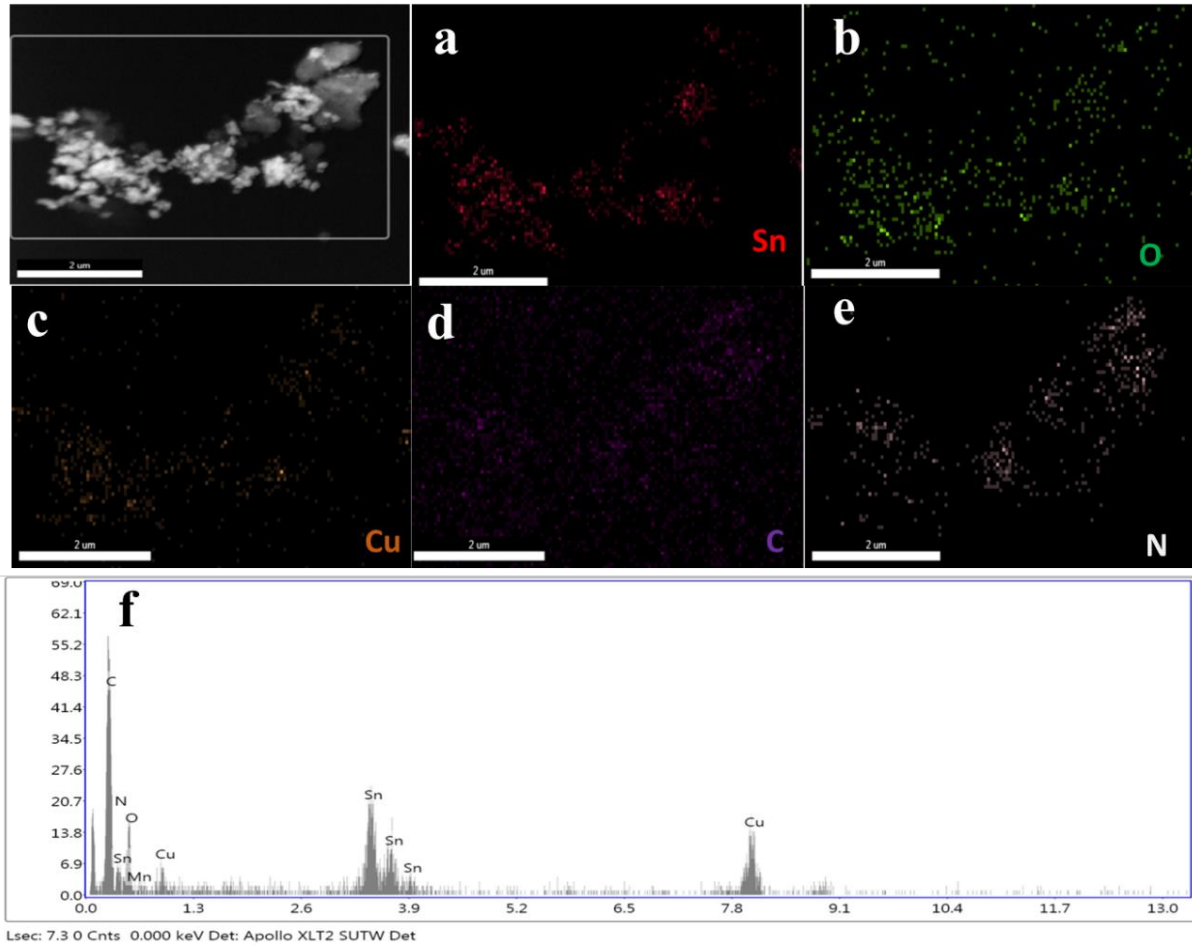Figure 5. Elemental Mapping (a-c) and EDX Analysis (d) of Cu Doped SnO_2

Figure 6. Elemental Mapping (a-e) and EDX Analysis (f) of Cu Doped SnO_2/g-C_3N_4

Chemical Composition Analysis

The XPS was utilized to evaluate the oxidation state and elemental composition of the components in the Cu doped SnO_2/g-C_3N_4. Spectral scan of the heterojunction revealed the presence of Sn, Cu, C, O, and N, thereby confirming the elemental composition of the Cu doped SnO_2/g-C_3N_4 (Fig 7a). For SnO_2, two distinct peaks were identified at 486.62 eV and 495.06 eV, representing Sn $3d_{5/2}$ and Sn $3d_{3/2}$, respectively, indicative of Sn^{4+} in SnO_2 (Fig 7 b)(Li et al., 2021). Oxygen exhibited a single peak at 531.7 eV, aligning with the framework oxygen of SnO_2 and Cu (Fig 7 c)(Akhundi & Habibi-Yangjeh, 2015a). Regarding Cu, two peaks with binding energies of Cu $2p_{3/2}$ and Cu $2p_{1/2}$ were noted at 932.4 and 952.4 eV, correspondingly, confirming the presence of Cu in Cu doped SnO_2/g-C_3N_4 (Fig 7 d)(Karikalan et al., 2017).

In the XPS spectrum of C 1s, three discernible peaks at 282.2, 284.5, and 287.6 were noted (Fig 7 e). The peaks at 284.5 and 282.2 eV were assigned to the graphitic C=C bond and CN group, respectively. Additionally, the C=N-C bond was represented by the peaks at 287.6 eV (Hamrouni et al., 2014). For the N 1s atom, three peaks at 398.1, 399.2, and 400.7 eV were observed (Fig 7 f), corresponding to C-N-C, N-(C)3, and C-N-H groups, respectively, in g-C_3N_4(Akhundi & Habibi-Yangjeh, 2015b). These XPS results provide valuable insights into the oxidation states and elemental configurations within the Cu doped SnO_2/g-C_3N_4 heterojunction nanocomposite.
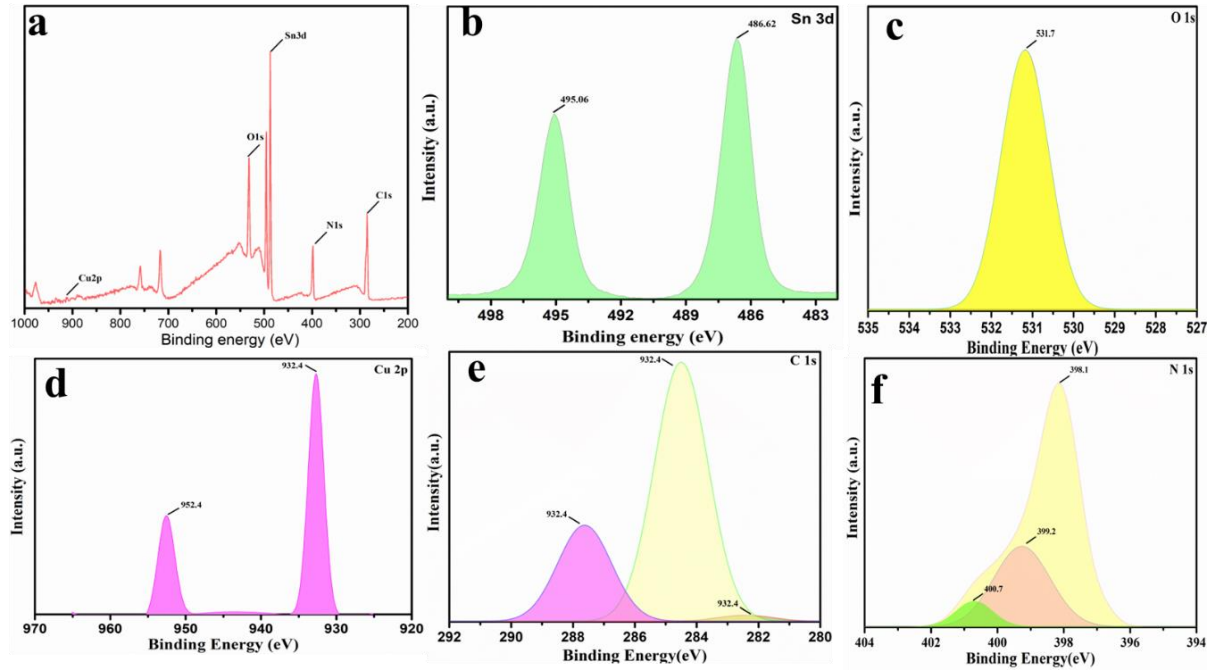
Figure 7. Full Scan XPS Spectra of Cu Doped SnO_2/g-C_3N_4 (a) and Narrow Scan Spectra of Sn 3d (b), O 1s (c), Cu 2p (d), C 1s (e) and N 1s (f)

Optical Analysis

In Fig 8, the UV-visible spectra of different materials, including synthesized pristine g-C_3N_4, the binary nanocomposite Cu doped SnO_2, and the Cu doped SnO_2/g-C_3N_4 heterojunction, are presented. Notably, the spectra exhibit distinct peaks that provide valuable insights into their optical properties. The absorption spectrum of pristine g-C_3N_4 reveals a prominent peak at 242.2 nm, which arises from electronic transitions within the carbon nitride structure containing s-triazine rings. Additionally, absorption bands 392 nm is observed, originating from charge transfer processes between the filled 2p orbitals of N and the 2p orbitals of C in g-C_3N_4. For the binary nanocomposite Cu doped SnO_2, there is an absorption band around 323 nm, which can be attributed to the strong light-absorbing capabilities of Sn^{2+} on the surface of SnO_2 within the visible light range. Regarding the instance of the Cu doped SnO_2/g-C_3N_4 heterojunction, distinctive absorbance peaks are observed at wavelengths around 342 nm. These shifts in absorbance are influenced by various factors, including changes in energy bandgap, alterations in surface properties, the presence of contaminant sites, and variations in oxygen content within the metal oxides.

The interaction between Cu doped SnO_2 and g-C_3N_4 in this heterojunction results in noticeable red-shifts in absorption and an increase in visible absorbance values. Consequently, this heterojunction exhibits exceptional photocatalytic potential when exposed to sunlight, as it features robust absorption bands within the visible light spectrum. The direct energy bandgap (Eg) of pristine g-C_3N_4, the binary nanocomposite Cu doped SnO_2, and the Cu doped SnO_2/g-C_3N_4 heterojunction was calculated using the equation

$\alpha h\nu = A (h\nu - Eg) n/2$

where α, h, ν, Eg, and A represent the absorption coefficient, Planck constant, frequency, energy bandgap, and a constant, respectively. the bandgap values for pure g-C$_3$N$_4$, the binary nanocomposite Cu doped SnO$_2$ and the Cu doped SnO$_2$/g-C$_3$N$_4$ heterojunction are calculated to be 2.68, 3.24, and 2.60 eV, respectively. The bandgap of the Cu doped SnO$_2$/g-C$_3$N$_4$ heterojunction is slightly lower than that of pristine g-C$_3$N$_4$ and the binary nanocomposite Cu doped SnO$_2$ indicating an increased ability to absorb visible light. As a result, the Cu doped SnO$_2$/g-C$_3$N$_4$ heterojunction is expected to exhibit superior photocatalytic performance compared to the individual materials. Furthermore, variations in the bandgap energy are observed due to the emergence of new doping levels within the heterojunction's lattice. These new levels facilitate efficient charge carrier generation and transitions from the valence band (VB) to the conduction band (CB), which leads to greater photo assisted catalytic activity(Singh et al., 2023).
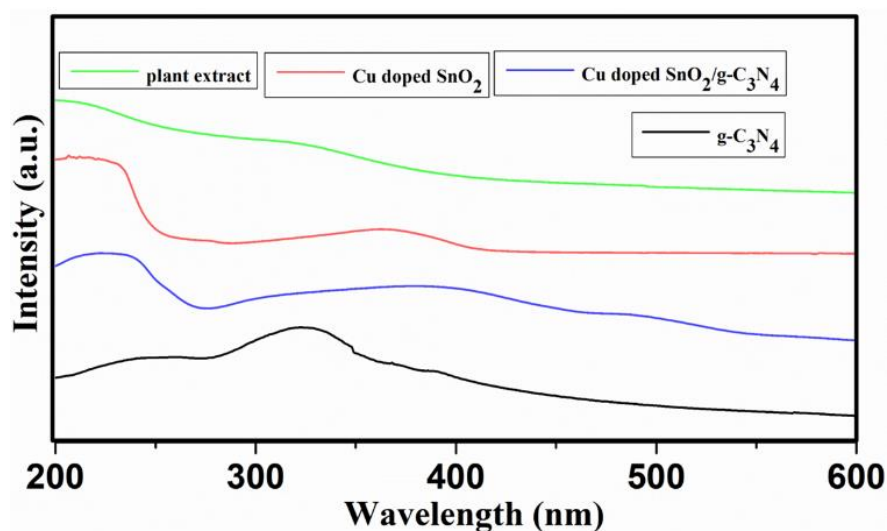

Figure 8. UV-Visible Absorption Spectra of *Murraya Paniculata* Plant Extract, g-C$_3$N$_4$, Cu Doped SnO$_2$ and Cu Doped SnO$_2$/g-C$_3$N$_4$

BET Analysis

Using a BET surface analyzer, we conducted an investigation into the surface structure, adsorption characteristics, and roughness properties of the Cu doped SnO$_2$/g-C$_3$N$_4$ heterojunction. As depicted in Fig 9 (a) and (b) it exhibits Type IV adsorption isotherms and H3 type hysteresis loops. The specific surface area per gram of adsorbent was determined to be approximately 12.91 m^2 g^{-1} for Cu doped SnO$_2$/g-C$_3$N$_4$ heterojunction. BJH (Barrett-Joyner-Halenda) evaluation was used to evaluate the porosity of the prepared nanocomposites. Fig illustrates the BJH plots for which revealed that the pore size distribution on the surface of Cu doped SnO$_2$/g-C$_3$N$_4$ heterojunction was uniform with the average pore diameters of the Cu doped SnO$_2$/g-C$_3$N$_4$ heterojunction measured 1.22 nm. Additionally, the average pore volume for Cu doped SnO$_2$/g-C$_3$N$_4$ semiconductor heterojunction was found to be 0.038 cm^{3}g^{-1}. These findings suggest that an effective fabrication process was employed, resulting in the excellent dispersion of Cu doped SnO$_2$ into the sheets of g-C$_3$N$_4$. This process also contributed to the stabilization of phytochemicals present in the plant extract, leading to an increased surface area and a reduction in particle size(Wang et al., 2009).
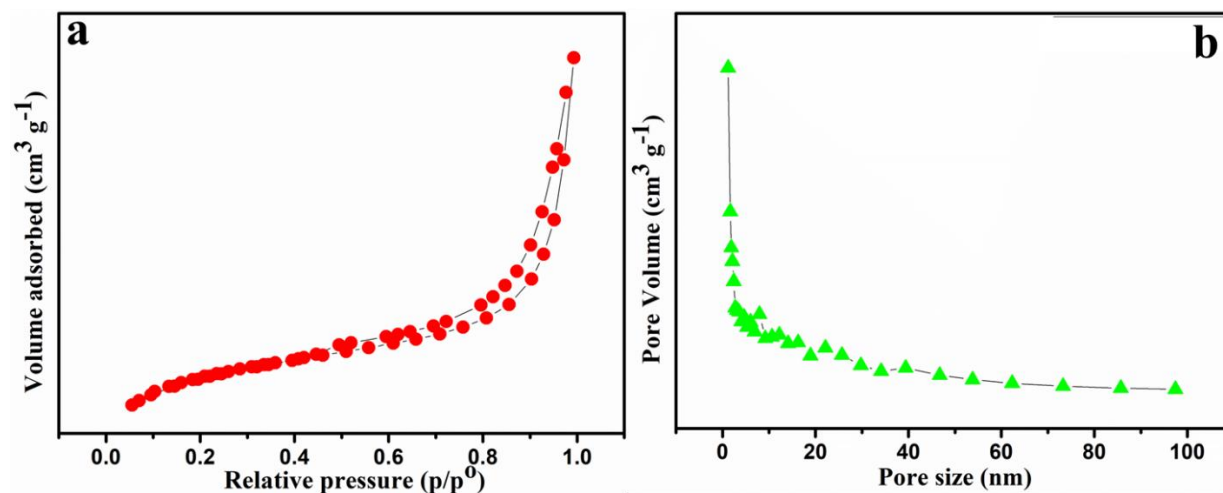
Figure 9. N2 Adsorption Desorption Isotherm (a) and BJH Plot of Cu Doped SnO$_2$/g-C$_3$N$_4$

Photo Assisted Catalytic Activity

We assessed the photocatalytic performance of pristine g-C$_3$N$_4$ sheets, the binary nanocomposite Cu doped SnO$_2$, and the Cu doped SnO$_2$/g-C$_3$N$_4$ heterojunction by studying their ability to degrade Malachite green (MG) dye under direct sunlight. In the absence of a photocatalyst, direct sunlight had a minimal effect on MG dye degradation, with only about 4.8% reduction. However, when the catalysts were introduced, they demonstrated the capacity to adsorb MG dye within 20 minutes of darkness, possibly due to interactions between the synthesized materials and the MG dye molecules. After being exposed for 100 minutes to direct daylight, the Cu doped SnO$_2$/g-C$_3$N$_4$ heterojunction showed noticeably greater photo assisted catalytic activity than the pristine g-C$_3$N$_4$ sheets and the binary nanocomposite Cu doped SnO$_2$.

The degradation percentages were found to be 35%, 40%, and 90% for pristine g-C$_3$N$_4$, the binary nanocomposite Cu doped SnO$_2$, and the Cu doped SnO$_2$/g-C$_3$N$_4$ heterojunction, respectively (Fig 10). To understand the kinetics of MG dye degradation, we examined the plots of C$_t$/C$_o$ vs. time and ln (C$_t$/C$_o$) vs. time, as depicted in Fig 11 (a) and (b) The data were best described by a pseudo-first-order kinetics model, with rate constants of 0.044 min^{-1}, 0.050 min^{-1}, and 0.222 min^{-1} for g-C$_3$N$_4$, the binary nanocomposite Cu doped SnO$_2$, and the Cu doped SnO$_2$/g-C$_3$N$_4$ heterojunction, respectively. Notably, the rate constant for the Cu doped SnO$_2$/g-C$_3$N$_4$ heterojunction was greater as compared to that of g-C$_3$N$_4$ and the binary nanocomposite Cu doped SnO$_2$.

This greater activity is attributed to the larger surface area and greater photosensitivity of the Cu doped SnO$_2$/g-C$_3$N$_4$ heterojunction. We also studied the impact of photocatalyst dosage on the decomposition rate of Malachite green dye by the Cu doped SnO$_2$/g-C$_3$N$_4$ heterojunction. Increasing the photocatalyst dosage from 10 mg to 30 mg significantly improved the degradation rate of MG dye, reaching 90% degradation after 100 minutes of direct sunlight exposure. However, further increasing the dosage to 40 mg and 50 mg brought about a minor decrease in the degradation %, showing 85% and 84%, respectively. The photo assisted degradation activity was evaluated using C$_t$/C$_o$ vs. time and ln (C$_t$/C$_o$) vs. time plots, revealing pseudo-first-order kinetics with rate constants of 0.057 min^{-1}, 0.087 min^{-1}, 0.229 min^{-1}, 0.190 min^{-1}, and 0.178 min^{-1} for 10, 20, 30, 40, and 50 mg of Cu doped SnO$_2$/g-

C_3N_4 heterojunction, respectively (Fig 12 a-b). It's important to note that excessively increasing the photocatalyst dosage may alter the internal structure of the material and potentially reduce electron-hole (e^-/h^+) interactions, leading to decreased photocatalyst efficiency. Additionally, we investigated the impact of pH on the photo assisted degradation of MG dye under direct sunlight in the presence of the Cu doped SnO_2/g-C_3N_4 heterojunction as a photocatalyst. The maximum photocatalytic activity was achieved at pH 11, resulting in a 92% degradation of MG dye. This improved performance is attributable to effective electron and hole transfer facilitated by the g-C_3N_4 network, as well as π-π interactions between g-C_3N_4 and MG dye molecules. Furthermore, the narrow band gap of the Cu doped SnO_2/g-C_3N_4 heterojunction contributes to its strong photocatalytic activity under direct sunlight. However, when the pH was decreased from 11 to 3, the rate of photo assisted degradation decreased from 92% to 29% (Fig 13). In the pH range of 3-5, the H+ ions buildup at the active sites of the Cu doped SnO_2/g-C_3N_4 heterojunction resulted in a positive charge and repulsion of the cationic organic compound. Conversely, at higher pH levels (10-11), the surface became more negatively charged, accelerating photodegradation efficiency.
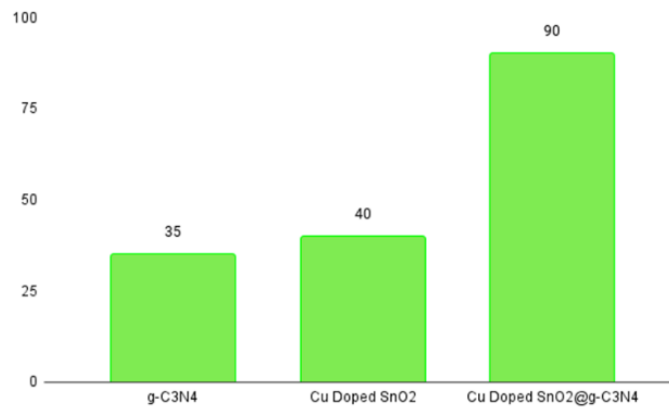

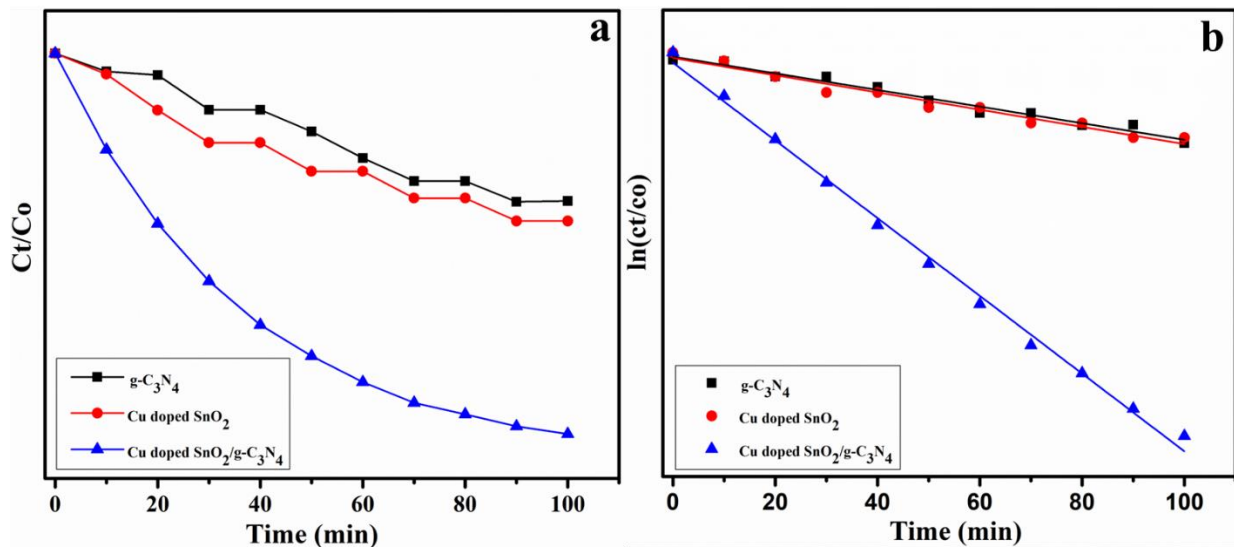Figure 10.Comparative Photodegradation Efficiency g-C_3N_4, Cu Doped SnO_2 and Cu Doped SnO_2/g-C_3N_4 as a Catalyst

Figure 11. Comparative Photodegradation Efficiency Ct/Co (a) and ln (Ct/Co) (b) of g-C_3N_4, Cu Doped SnO_2 and Cu Doped SnO_2/g-C_3N_4 as a Catalyst
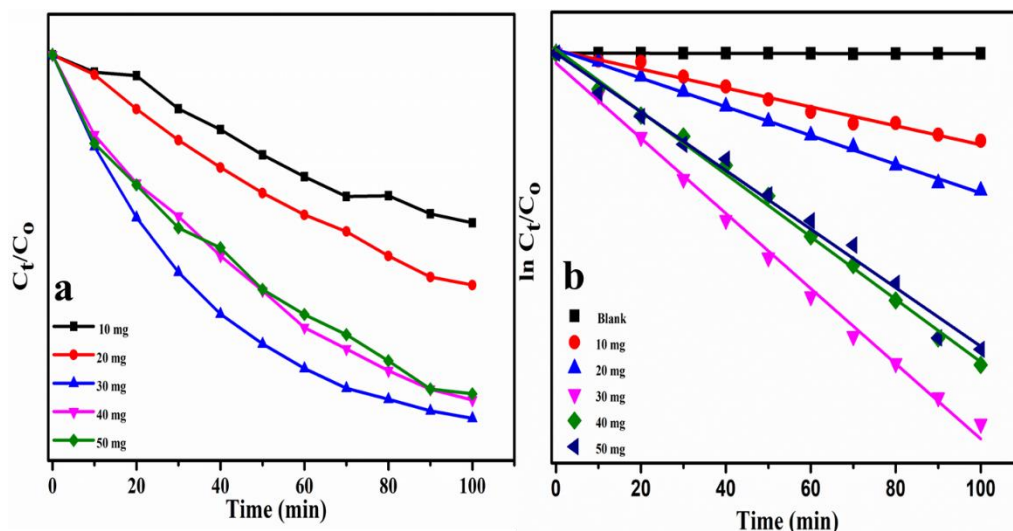
Figure 12. Photocatalytic Degradation of Dye MG by Cu doped SnO_2/g-C_3N_4 at Different Doses (a) and Kinetic plot of Photocatalytic Degradation of Dye MG by Cu Doped SnO_2/g-C_3N_4 (b)
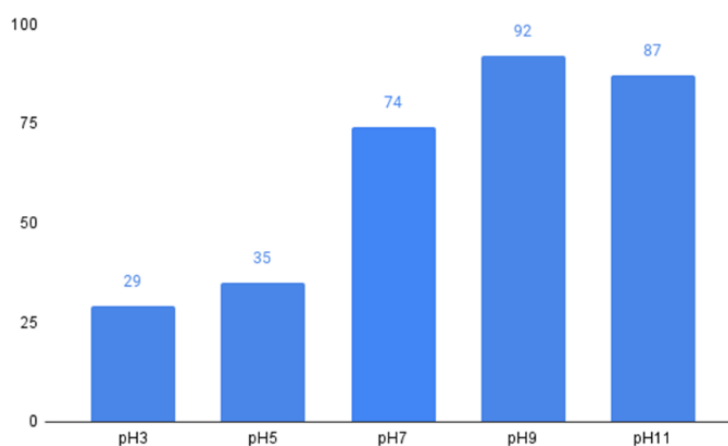

Figure 13. Photocatalytic degradation of MG at different pH by Cu doped SnO_2/g-C_3N_4

COD Measurement

The complete breakdown of dye Malachite green (MG) into its constituent components, namely, carbon dioxide (CO_2) and water (H_2O), could not be definitively confirmed through UV-Visible spectrophotometer analysis. Consequently, it is of utmost importance to employ Chemical Oxygen Demand (COD) analysis to gain a deeper understanding of the mineralization process of dye MG. COD analysis serves to quantify the amount of oxygen required to oxidize various organic substances present in water, and it was carried out using the dichromate reflux method. The initial concentrations of dye MG and the photocatalyst loading were standardized at 10 mg/L and 50 mg, respectively.

Table 1 presents a summary of the percentage decrease in COD, which illustrates the comprehensive mineralization of the harmful dye pollutant. This COD evaluation has a vital function in confirming the successful conversion of dye MG into environmentally benign components during the photocatalytic degradation process.

Table 1. COD Measurements

S.NO.	CV	% Decrease in COD
1	Prior to Sunlight exposure	5%
2	Followed by 20 minutes of exposure	24%
3	Followed by 40 minutes of exposure	80%
4	Followed by 60 minutes of exposure	92%

LC-MS Analysis

The photodegradation mechanism of the dye MG using the synthesized heterojunction Cu doped SnO_2/g-C_3N_4 as a photocatalyst was investigated through the LC-MS technique. This analytical approach facilitated the identification of various degradation products formed during the degradation process of the MG dye. In Fig 14 (a) and (b), the Liquid Chromatography-MS spectra of the untreated and treated MG dye by the heterojunction Cu doped SnO_2/g-C_3N_4 photocatalyst are presented. The Liquid Chromatography -MS spectrum of the untreated MG dye exhibited a characteristic peak at m/z=329. In contrast, the LC-MS spectrum of the treated MG dye by the heterojunction Cu doped SnO_2/g-C_3N_4 revealed peaks at m/z=358, 318, 243, 198, 135, and 112. These peaks corresponded to the degraded products $C_{23}H_{25}ClN_2$, $C_{23}H_{25}N_2^{2+}$, $C_{19}H_{18}N_2$, $C_{13}H_{11}NO$, $C_8H_{11}NO$, and $C_4H_4O_4$, respectively (Kumar et al., 2022; Verma et al., 2020). The potential degradation mechanism of the MG dye is illustrated in Fig 15.
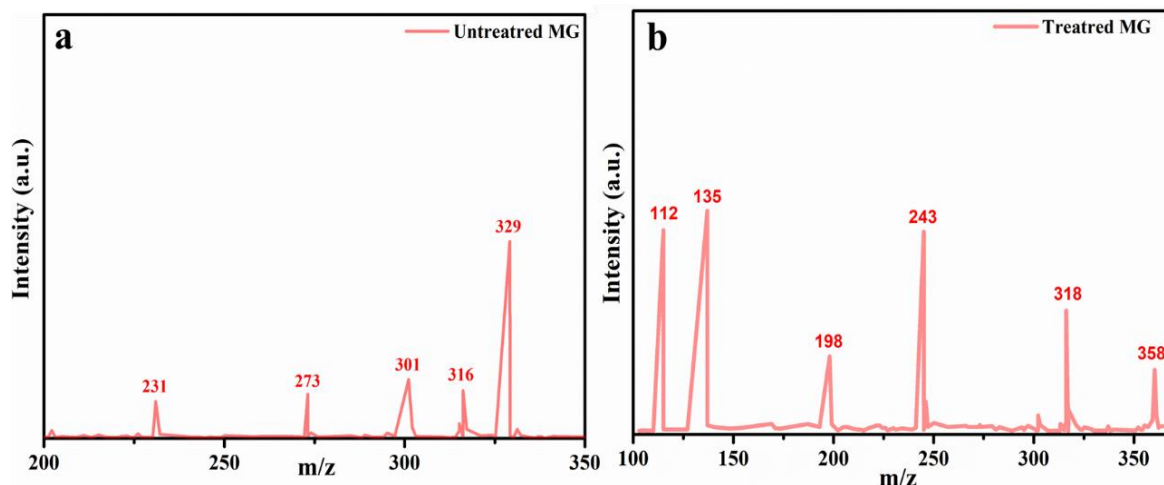

Figure 14. LC-MS Peaks of Untreated Dye MG (a), Treated Dye MG (b)

Radical Scavenger Experiment

The photo assisted catalytic mechanism encompass a variety of active species, which include photo generated electrons (e-), superoxide radicals ($^\cdot O_2{}^-$), holes (h^+) and hydroxyl radicals ($^\cdot OH$). To gain deeper insights into the contributions of these photocatalytic active species in the degradation of dye Malachite green (MG), we introduced several scavengers: isopropanol (IPA), p-benzoquinone (BQ), and Na2 EDTA.

These scavengers were used to specifically trap $^{\bullet}OH$, $^{\bullet}O_2^{\,-}$, and h^+, respectively, each at a concentration of 0.01 M within an aqueous solution. In a general sense, these scavengers were incorporated into the reaction mixture containing both dye MG and the photocatalyst. Subsequently, we evaluated the catalytic performance with the existence of these radical scavengers. The introduction of radical scavengers significantly impacted the decomposition rates of dye MG, as depicted in Fig 16. When IPA, BQ, and Na_2 EDTA were included in the reaction mixture, the inhibition of the dye MG degradation rate followed this order: BQ > Na2 EDTA > IPA. This suggests that h^+ and $^{\bullet}O_2^{\,-}$ species exert a more substantial influence on the photodegradation process of dye MG, while $^{\bullet}OH$ plays a comparatively minor role in the degradation process.

In particular, the addition of Na_2 EDTA and BQ led to a notable deceleration in the decomposition rate, underscoring the pronounced impact of h^+ and $^{\bullet}O_2^{\,-}$ radicals on the decomposition of dye MG. For a visual depiction of the possible electron transfer mechanism involved in the decomposition of dye MG by the Cu doped SnO_2/g-C_3N_4 heterojunction under solar light, please refer to Scheme 1. When subjected to solar light irradiation, g-C_3N_4 and Cu doped SnO_2 generate photoinduced electrons (e-) and holes (h+).

Since the conduction band (CB) of g-C_3N_4 (-1.17 eV vs. NHE) is more negatively charged than the CB of Cu doped SnO_2 (-0.72 eV vs. NHE), the excited electrons from the CB of g-C_3N_4 can easily migrate to the CB of Cu doped SnO_2. This facilitates the transfer of photoexcited holes (h^+) from the valence band (VB) of Cu doped SnO_2 to the VB of g-C_3N_4, effectively preventing electron-hole recombination. The photoelectrons then engage with O_2 to generate $^{\bullet}O_2^{\,-}$, while the photogenerated holes (h^+) react with the dye MG, causing oxidation. Consequently, these active radicals $^{\bullet}O_2^{\,-}$ and h^+ are the primary contributors to the photodegradation of dye MG.
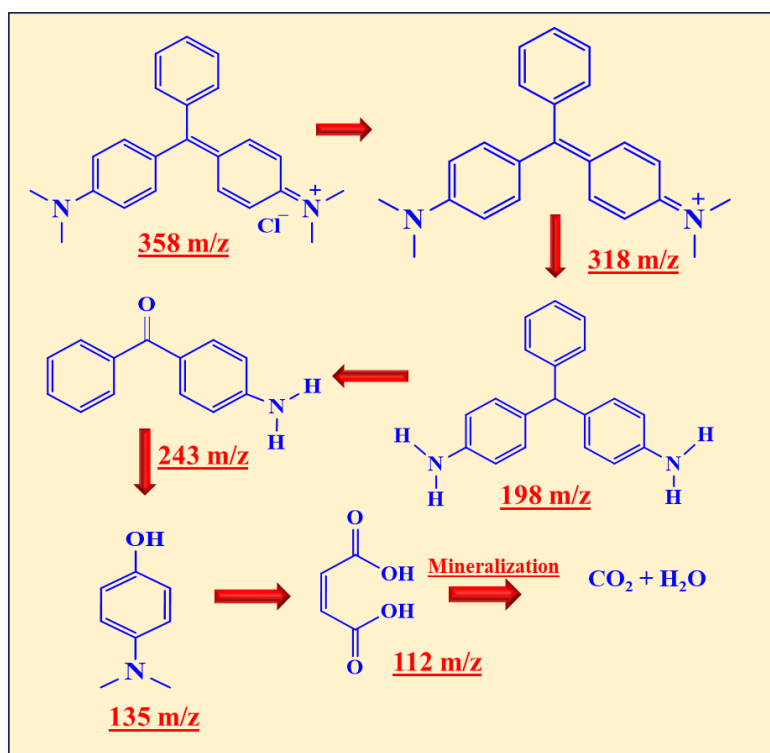

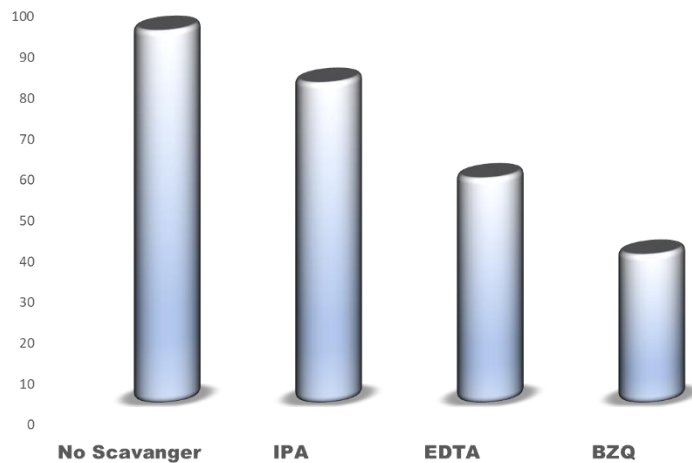Figure 15. Possible Mechanism for Photocatalytic Degradation of Dye MG

Figure 16. Effect of Scavengers on Photocatalytic Degradation of Dye MG by Cu Doped $SnO_2/g\text{-}C_3N_4$

Recyclability Studies

We subjected the Cu doped $SnO_2/g\text{-}C_3N_4$ heterojunction to a rigorous assessment of its recyclability for the degradation of dye Malachite green (MG) over four consecutive cycles. In each cycle, the Cu doped $SnO_2/g\text{-}C_3N_4$ heterojunction underwent a meticulous process that included extraction from the reaction solution, thorough washing, drying at 80°C, and subsequent reintegration into the photocatalytic process. The results unveiled a minor reduction in the photocatalytic degradation efficiency during the third cycle, while the first and second cycles exhibited no substantial decline, as depicted in Fig 17. Furthermore, we scrutinized the XRD pattern after the completion of four cycles, as demonstrated in Fig 18. This in-depth analysis showed no discernible alterations in the shape or crystalline phase structure of the Cu doped $SnO_2/g\text{-}C_3N_4$ heterojunction, indicating an impressive level of stability. These findings collectively indicate that the Cu doped $SnO_2/g\text{-}C_3N_4$ heterojunction is highly likely to possess exceptional stability and reliability for the photodegradation of dye MG over multiple cycles.

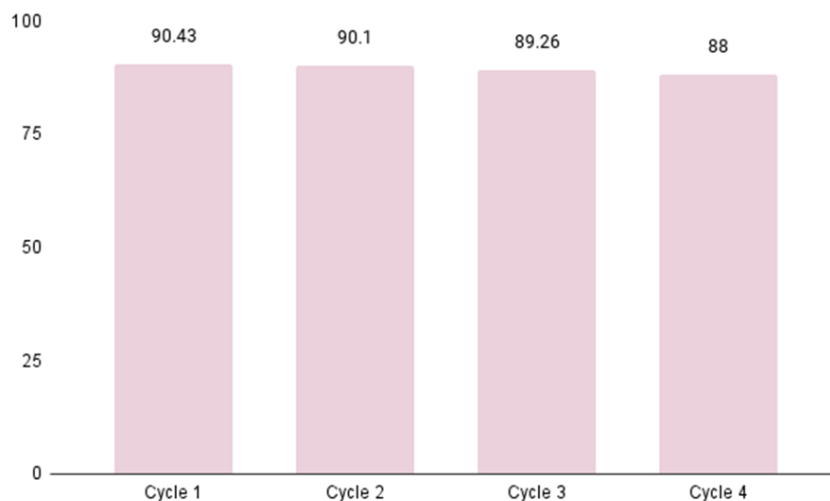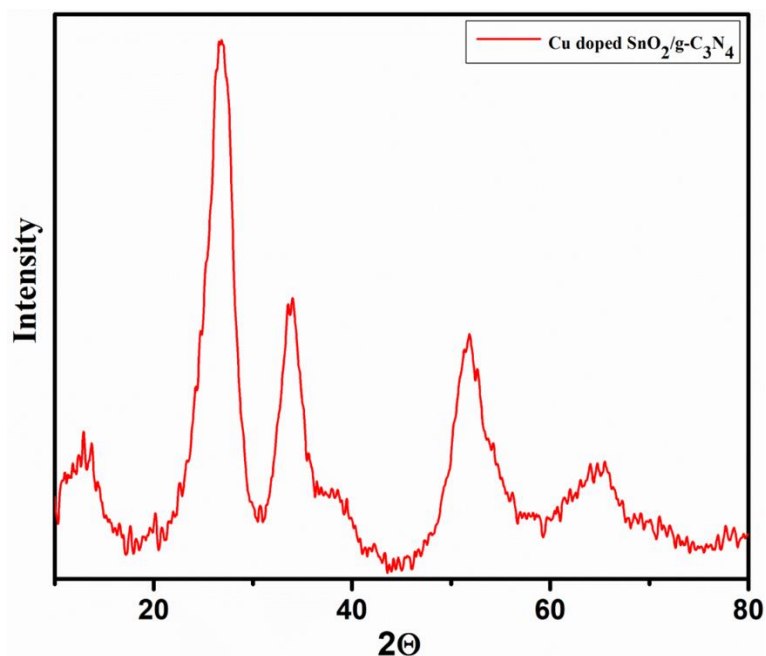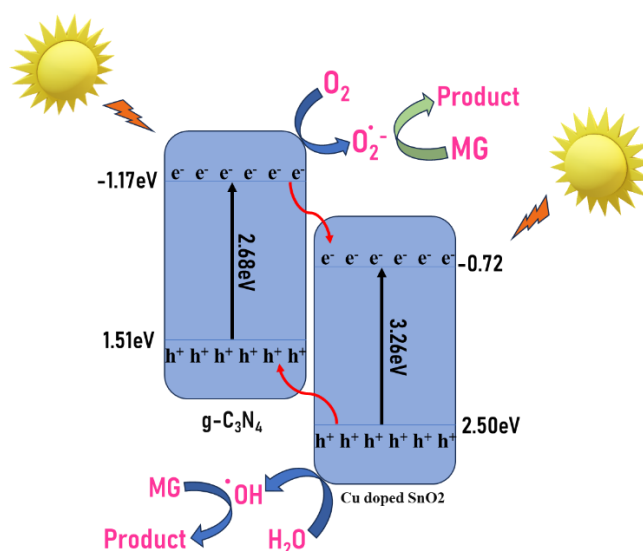Figure 17. Recyclability test of Photocatalytic Degradation of Dye MG by Cu Doped $SnO_2/g\text{-}C_3N_4$

Figure 18. XRD Pattern of Used Heterojunction Cu Doped SnO$_2$/g-C$_3$N$_4$

Scheme 1. Plausible Mechanism of Photocatalytic Degradation of Dye MG by Cu Doped SnO$_2$/g-C$_3$N$_4$

Conclusion

In this work, we successfully synthesized a nanocomposite of Cu doped SnO$_2$ and a heterojunction Cu doped SnO$_2$/g-C$_3$N$_4$ using a one-pot green synthesis approach. *Murraya paniculata* leaves extract played a crucial role as a stabilizing and reducing agent throughout the synthesis process, highlighting the efficacy of green synthesis as an environmentally friendly, cost-effective, and biocompatible method for nanomaterial production. XRD results disclosed the spherical morphology of the particles, with mean grain sizes of 2.18 nm for Cu doped SnO$_2$/g-C$_3$N$_4$ and 2.14 nm for Cu doped SnO$_2$/g-C$_3$N$_4$. High-resolution TEM unveiled that the synthesized Cu doped SnO$_2$ comprised very small-sized spherical nanoparticles that agglomerated in the presence of adsorbed phytochemicals,

forming larger aggregates. The heterojunction Cu doped SnO_2/g-C_3N_4 exhibited a 2-D sheeted structure of g-C_3N_4, acts as a translucent sheet that captured sphere-shaped Cu doped SnO_2. The existence of Sn, Cu, C, N, and O in both nanocomposites was further confirmed through XPS, EDX spectroscopy (EDAX), and elemental mapping. According to UV-Visible spectra, the heterojunction Cu doped SnO_2/g-C_3N_4 and the nanocomposite Cu doped SnO_2 exhibited band gap energies of 2.60 and 3.24 eV, correspondingly. The catalytic prowess of the fabricated heterojunction Cu doped SnO_2/g-C_3N_4 was demonstrated in the photodegradation of the dye MG under sunlight irradiation. Remarkably, the heterojunction Cu doped SnO_2/g-C_3N_4 displayed an outstanding degradation efficiency of 90%, significantly surpassing the nanocomposite Cu doped SnO_2/g-C_3N_4 with a degradation percentage of 40% under identical reaction conditions. Kinetic analysis indicated a pseudo-first-order reaction for both nanocomposites, with the active radicals involved in the photodegradation identified as $^{\bullet}O_2^{\,-}$ and h^+.

References

Akhundi, A., Badiei, A., Ziarani, G. M., Habibi-Yangjeh, A., Munoz-Batista, M. J., & Luque, R. (2020). Graphitic carbon nitride-based photocatalysts: toward efficient organic transformation for value-added chemicals production. *Molecular Catalysis*, *488*, 110902.

Akhundi, A., & Habibi-Yangjeh, A. (2015a). A simple large-scale method for preparation of g-C3N4/SnO2 nanocomposite as visible-light-driven photocatalyst for degradation of an organic pollutant. *Materials Express*, *5*(4), 309-318.

Akhundi, A., & Habibi-Yangjeh, A. (2015b). Ternary g-C3N4/ZnO/AgCl nanocomposites: synergistic collaboration on visible-light-driven activity in photodegradation of an organic pollutant. *Applied Surface Science*, *358*, 261-269.

Alalm, M. G., Djellabi, R., Meroni, D., Pirola, C., Bianchi, C. L., & Boffito, D. C. (2021). Toward scaling-up photocatalytic process for multiphase environmental applications. *Catalysts*, *11*(5), 562.

Bamsaoud, S. F., Rane, S., Karekar, R., & Aiyer, R. (2011). Nano particulate SnO2 based resistive films as a hydrogen and acetone vapour sensor. *Sensors and Actuators B: Chemical*, *153*(2), 382-391.

Chen, D., Huang, S., Huang, R., Zhang, Q., Le, T.-T., Cheng, E., Yue, R., Hu, Z., & Chen, Z. (2019). Construction of Ni-doped SnO2-SnS2 heterojunctions with synergistic effect for enhanced photodegradation activity. *Journal of hazardous materials*, *368*, 204-213.

Goswami, Y., Begzaad, S., & Kaundal, J. B. (2022). Highly luminescent Cu doped SnO2 nanocomposites and their photocatalytic application as excellent methylene dye removal. *Journal of Advanced Scientific Research*, *13*(04), 94-103.

Hamrouni, A., Moussa, N., Parrino, F., Di Paola, A., Houas, A., & Palmisano, L. (2014). Sol–gel synthesis and photocatalytic activity of ZnO–SnO2 nanocomposites. *Journal of Molecular Catalysis A: Chemical*, *390*, 133-141.

Hong, N. H., Chikoidze, E., & Dumont, Y. (2009). Ferromagnetism in laser ablated ZnO and Mn-doped ZnO thin films: A comparative study from magnetization and Hall effect measurements. *Physica B: Condensed Matter*, *404*(21), 3978-3981.

Jiang, L., Yuan, X., Zeng, G., Wu, Z., Liang, J., Chen, X., Leng, L., Wang, H., & Wang, H. (2018). Metal-free efficient photocatalyst for stable visible-light photocatalytic degradation of refractory pollutant. *Applied*

Catalysis B: Environmental, *221*, 715-725.

Jin, H., Xu, Y., Pang, G., Dong, W., Wan, Q., Sun, Y., & Feng, S. (2004). Al-doped SnO2 nanocrystals from hydrothermal systems. *Materials chemistry and physics*, *85*(1), 58-62.

Kapilashrami, M., Xu, J., Ström, V., Rao, K. V., & Belova, L. (2009). Transition from ferromagnetism to diamagnetism in undoped ZnO thin films. *Applied Physics Letters*, *95*(3).

Karikalan, N., Karthik, R., Chen, S.-M., Karuppiah, C., & Elangovan, A. (2017). Sonochemical synthesis of sulfur doped reduced graphene oxide supported CuS nanoparticles for the non-enzymatic glucose sensor applications. *Scientific reports*, *7*(1), 2494.

Kasar, R., Deshpande, N., Gudage, Y., Vyas, J., & Sharma, R. (2008). Studies and correlation among the structural, optical and electrical parameters of spray-deposited tin oxide (SnO2) thin films with different substrate temperatures. *Physica B: Condensed Matter*, *403*(19-20), 3724-3729.

Kolmakov, A., Zhang, Y., & Moskovits, M. (2003). Topotactic thermal oxidation of Sn nanowires: intermediate suboxides and core− shell metastable structures. *Nano Letters*, *3*(8), 1125-1129.

Kumar, J. V., Ajarem, J. S., Allam, A. A., Manikandan, V., Arulmozhi, R., & Abirami, N. (2022). Construction of SnO2/g-C3N4 an effective nanocomposite for photocatalytic degradation of amoxicillin and pharmaceutical effluent. *Environmental Research*, *209*, 112809.

Kumar, V., Rajaram, P., & Goswami, Y. (2016). Sol gel synthesis of SnO2/CdSe nanocomposites and their optical structural and morphological characterizations. *Optik*, *127*(5), 2490-2494.

Kumar, V., Rajaram, P., & Goswami, Y. (2017). Sol–gel synthesis of SnO 2/CdS heterostructures using various Cd: S molar ratio solutions and its application in photocatalytic degradation of organic dyes. *Journal of Materials Science: Materials in Electronics*, *28*, 9024-9031.

Lai, W. (2017). Pesticide use and health outcomes: Evidence from agricultural water pollution in China. *Journal of environmental economics and management*, *86*, 93-120.

Lee, S.-Y., & Park, B.-O. (2006). Structural, electrical and optical characteristics of SnO2: Sb thin films by ultrasonic spray pyrolysis. *Thin solid films*, *510*(1-2), 154-158.

Li, D., Huang, J., Li, R., Chen, P., Chen, D., Cai, M., Liu, H., Feng, Y., Lv, W., & Liu, G. (2021). Synthesis of a carbon dots modified g-C3N4/SnO2 Z-scheme photocatalyst with superior photocatalytic activity for PPCPs degradation under visible light irradiation. *Journal of hazardous materials*, *401*, 123257.

Li, S., Liu, Z., Qu, Z., Piao, C., Liu, J., Xu, D., Li, X., Wang, J., & Song, Y. (2020). An all-solid-state Z-scheme NaNbO3-Au-Sn3O4 photocatalyst for effective degradation of carbofuran under sunlight irradiation. *Journal of Photochemistry and Photobiology A: Chemistry*, *389*, 112246.

Mishra, R., Kushwaha, A., & Sahay, P. P. (2014). Influence of Cu doping on the structural, photoluminescence and formaldehyde sensing properties of SnO 2 nanoparticles. *RSC advances*, *4*(8), 3904-3912.

Mohanta, D., & Ahmaruzzaman, M. (2016). Tin oxide nanostructured materials: an overview of recent developments in synthesis, modifications and potential applications. *RSC advances*, *6*(112), 110996-111015.

Mohanta, D., & Ahmaruzzaman, M. (2021). Facile fabrication of novel Fe3O4-SnO2-gC3N4 ternary nanocomposites and their photocatalytic properties towards the degradation of carbofuran. *Chemosphere*, *285*, 131395.

Raha, S., & Ahmaruzzaman, M. (2020). Enhanced performance of a novel superparamagnetic g-

C3N4/NiO/ZnO/Fe3O4 nanohybrid photocatalyst for removal of esomeprazole: Effects of reaction parameters, co-existing substances and water matrices. *Chemical Engineering Journal*, *395*, 124969.

Sagadevan, S., Chowdhury, Z. Z., Johan, M., Bin, R., Aziz, F. A., Roselin, L. S., Podder, J., Lett, J. A., & Selvin, R. (2019). Cu-doped SnO2 nanoparticles: synthesis and properties. *Journal of nanoscience and nanotechnology*, *19*(11), 7139-7148.

Singh, K. B., Upadhyay, D. D., Gautam, N., Gautam, A., & Pandey, G. (2023). Sonochemical reassembling of Acacia nilotica bark extract mediated Mg doped WO3@ g-C3N4 ternary nanocomposite: A robust nanophotocatalyst. *Journal of Photochemistry and Photobiology A: Chemistry*, *441*, 114739.

Verma, M., Singh, K. P., & Kumar, A. (2020). Reactive magnetron sputtering based synthesis of WO3 nanoparticles and their use for the photocatalytic degradation of dyes. *Solid State Sciences*, *99*, 105847.

Wang, X., Maeda, K., Thomas, A., Takanabe, K., Xin, G., Carlsson, J. M., Domen, K., & Antonietti, M. (2009). A metal-free polymeric photocatalyst for hydrogen production from water under visible light. *Nature materials*, *8*(1), 76-80.

Wen, Y., Feng, M., Zhang, P., Zhou, H.-C., Sharma, V. K., & Ma, X. (2021). Metal organic frameworks (MOFs) as photocatalysts for the degradation of agricultural pollutants in water. *ACS ES&T Engineering*, *1*(5), 804-826.

Zhao, C., Gong, H., Niu, G., & Wang, F. (2020). Ultrasensitive SO2 sensor for sub-ppm detection using Cu-doped SnO2 nanosheet arrays directly grown on chip. *Sensors and Actuators B: Chemical*, *324*, 128745.

Author Information

Snigdha Dwivedi

https://orcid.org/0009-0003-2375-2854

Babasaheb Bhimrao Ambedkar University

Department of Chemistry

Lucknow-226025

India

Contact e-mail: *snigdha.vatsa1994@gmail.com*

Gajanan Pandey

https://orcid.org/0000-0002-9568-3486

Babasaheb Bhimrao Ambedkar University

Department of Chemistry

Lucknow-226025

India